文章编号：1001-9014(XXXX)XX-0001-07

DOI:10.11972/j.issn.1001-9014.XXXX.XX.001

Visible to near-infrared photodetector based on organic semiconductor single crystal

LI Xiang[1,2], HU Jin-Han[2,3], ZHONG Zhi-Peng[2], CHEN Yu-Zhong[2], WANG Zhi-Qiang[2], SONG Miao-Miao[1], WANG Yang[2], ZHANG Lei[1*], LI Jian-Feng[3*], HUANG Hai[2*]

(1. School of Mathematics and Physics, Lanzhou Jiaotong University, Lanzhou 730070, China;
2. State Key Laboratory of Photovoltaic Science and Technology, Shanghai Frontiers Science Research Base of Intelligent Optoelectronic and Perception, Institute of Optoelectronic and Department of Material Science, Fudan University, Shanghai 200433, China;
3. School of Materials Science and Engineering, Lanzhou Jiaotong University, Lanzhou 730070, China)

Abstract: Organic semiconductor materials have shown unique advantages in the development of optoelectronic devices due to their ease of preparation, low cost, lightweight, and flexibility. In this work, we explored the application of the organic semiconductor Y6-1O single crystal in photodetection devices. Firstly, Y6-1O single crystal material was prepared on a silicon substrate using solution droplet casting method. The optical properties of Y6-1O material were characterized by polarized optical microscopy, fluorescence spectroscopy, etc., confirming its highly single crystalline performance and emission properties in the near-infrared region. Phototransistors based on Y6-1O materials with different thicknesses were then fabricated and tested. It was found that the devices exhibited good visible to near-infrared photoresponse, with the maximum photoresponse in the near-infrared region at 785 nm. The photocurrent on/off ratio reaches 10^2, and photoresponsivity reaches 16 mA/W. It was also found that the spectral response of the device could be regulated by gate voltage as well as the material thickness, providing important conditions for optimizing the performance of near-infrared photodetectors. This study not only demonstrates the excellent performance of organic phototransistors based on Y6-1O single crystal material in near-infrared detection but also provides new ideas and directions for the future development of infrared detectors.

Key words: near-infrared photodetector, organic semiconductor, Y6-1O single crystal, spectral response

基于有机半导体单晶的可见至近红外光电探测器

李 湘[1,2], 胡金瀚[2,3], 钟志鹏[2], 陈于中[2], 王志强[2], 宋苗苗[1], 王 洋[2], 张 磊[1*], 李建丰[3*], 黄 海[2*]

(1. 兰州交通大学数理学院,甘肃 兰州 730070;
2. 复旦大学光电研究院、材料科学系,上海智能光电与感知前沿科学研究基地,光伏科学与技术国家重点实验室,上海 200433;
3. 兰州交通大学材料科学与工程学院,甘肃 兰州 730070)

摘要:有机半导体材料因其易于制备、低成本、质量轻、可柔性弯折等特点,在光电子器件开发中表现出了独特的优势。本文探究了有机半导体晶体材料Y6-1O材料的在光探测器件中的应用。首先利用溶液滴铸法在硅基衬底上制备Y6-1O单晶材料,并利用偏光显微镜、荧光光谱等方法表征了Y6-1O材料的光学性质,验证其高度单晶结晶性能以及近红外区的发光性能。接着制备了基于不同厚度Y6-1O材料的场效应晶体管器件,

Received date: 2024-04-07, **revised date**: 2024-04-29 **收稿日期**:2024-04-07,**修回日期**:2024-04-29

Foundation items: Supported by the National Key Research and Development Program of China (2021YFB2012601); National Natural Science Foundation of China (12204109); Science and Technology Innovation Plan of Shanghai Science and Technology Commission (21JC1400200); Higher Education Industry Support Program of Gansu Province (2022CYZC-06); Part of the experimental work has been carried out in Fudan Nanofabrication Laboratory.

Biography: LI Xiang (1998-), female (Tujia), Hunan, master, Research area involves Photoelectric detection of semiconductor materials. E-mail: 24110300017@m.fudan.edu.cn.

* **Corresponding authors**: E-mail: ZHANG Lei (zl_lzjtu@126.com); LI Jian-Feng (ljfpyc@163.com); HUANG Hai (huangh@fudan.edu.cn);

通过光电性能测试,发现器件表现出良好的可见至近红外光响应,器件的光谱响应峰值在785 nm的近红外区,光开关比达10^2,光响应率可达16 mA/W。还发现器件的光谱响应可受栅压调控,并且与材料厚度等因素相关,为优化调节近红外光电探测器性能提供了重要条件。本研究不仅展示了基于Y6-1O单晶材料的有机光电晶体管在近红外探测上的优异性能,也为未来发展红外探测器提供了新的思路和方向。

关 键 词:近红外光探测器;有机半导体;Y6-1O单晶;光谱响应

中图分类号:TN383 **文献标识码**:A

Introduction

Organic semiconductors have attracted increasing attentions in the application of modern electronics and optoelectronics because of their outstanding optoelectronic properties, flexibility, low cost and solution-processable advantages[1-6]. In comparison with inorganic materials, organic semiconductors are lightweight and easily fabricated over large areas, showing unique potential in the fields of wearable electronics[7-10], flexible display screens[11-15], photodetectors[16-19], and photovoltaic devices[20-25].

Recent advancements in the design of narrow-bandgap conjugated small molecules and polymers have led to the development of high-performance organic semiconductor materials, broading their application spectrum further[26-30]. For instance, the emergence of Y-series nonfullerene acceptors has significantly boosted the performance of organic solar cells, whose power conversion efficiency is approaching to 20%[31-37]. As one of the most representatives, Y6 processes banana-curved molecule structure, and by replacing one outer alkyl chain in Y6 with an alkoxy chain leading to the structure of Y6-1O. It has a tighter molecular packing in thin film and can be easily grown into single crystals, leading to the excellent electronic transport properties. Y. Chen *et al*. has shown the fabrication of the Y6-1O single crystal on silicon substrate through the droplet casting method. And the resulting n-type organic field effect transistors based on Y6-1O has shown high performance with high on/off ratio and extraordinary electron mobility[38]. Moreover, the ultraviolet-vis-near infrared (UV-vis-NIR) absorption spectra has shown that Y6-1O has a high absorption efficiency in the near-infrared (NIR)[39, 40], with a bandgap estimated to be approximately 1.33 eV[41], indicating its high potential for NIR photodetection applications. However, studies on the photodetection application of Y6-1O single crystal are still absent.

In this work, we fabricated a phototransistor based on the Y6-1O single crystal and had systematically studied its photoresponse from visible to the NIR. We found that the photodetector based on Y6-1O shows excellent photoresponsivity with low dark current. And the maximum optical photoresponse occurs at 785 nm in the NIR region, which aligns well with the photoluminescence spectroscopy of the Y6-1O. Furthermore, we observed that the photoresponsivity increases with the thickness of Y6-1O single crystals. These results shown the organic semiconductor single crystal Y6-1O could function as a promising infrared photodetector in the future organic optoelectronics. It can not only contribute to the advancements in infrared detection technology, but also paves the way for novel application of organic semiconductor materials in the field of photodetection.

1 Experiments

The Y6-1O single crystals were made through the droplet casting method on the heavily p-doped silicon substrate with a 285 nm-thick oxidation layer. In this process, 20 μL of 0.5 mg/ml of Y6-1O xylene solution was dispensed onto the clean substrate, and placed in the N_2 glove box for 12 hours to allow solvent evaporation. Subsequently, Y6-1O single crystal with suitable length and thickness were selected through the optical microscope, and micro sized metal mask were used to fabricate the electrode. Au electrodes of 60 nm-thick was deposited through a thermal evaporation system at a rate of 2 angstroms per second. The photoluminescence (PL) spectra were measured using the laser micro confocal spectrometer (Renishaw, 532 nm excitation laser). Optoelectrical characterization of the Y6-1O based phototransistor was conducted using a Keithley 4200A-SCS parameter analyzer in the lakeshore probe station. Laser diode operating at different wavelengths were used as the optical lightsource to measure the photoresponse of the device.

2 Results and discussions

The molecule structure of Y6-1O is shown in Fig. 1(a), it smartly combines the electron-pulling core and the electron-pushing side chain, and by adjusting the delicate balance of these structures, leading to a highly efficient conversion of the photons. The single crystal of Y6-1O grown on Si/SiO_2 substrates is typically in a nanoribbon shape, with a length of tens micrometers. The photograph of Y6-1O nanoribbon is taken with a polarized optical microscopy. As it can be seen in Fig. 1(b), it demonstrates the alternating between light and dark while changing the polarization of the incident light. This is because the birefringence nature of the Y6-1O single crystal, revealing the single crystalline structure of the nanoribbon.

The phototransistors based on the Y6-1O single crystal with different thicknesses were fabricated on the Si/SiO_2 substrates. Fig. 1(c) and 1(d) the scanning electron microscopy (SEM) and atomic force microscopy (AFM) of the device, respectively. The channel length of Y6-1O phototransistor is approximately 15 μm. The thickness profile of the devices with different thicknesses, 108 nm, 660 nm and 1060 nm are shown in Fig. 1(e). The AFM tomography shows the Y6-1O single crys-

tals process flat surface with minimum roughness, indicating their highly crystal quality. It's worthy to note that as the thickness of the Y6-1O nanoribbon changes, the width of single crystal also varies. To study the optoelectronic properties of the Y6-1O single crystal, we firstly measured the PL properties of the single crystal in different thicknesses. As depicted in Fig. 1(f), the PL spectra of the Y6-1O show a high emission peak at approximately 910 nm, indicating its bandgap falls within the NIR region. Another weak emission peak locates in the visible light region, about 610 nm. These results suggests the Y6-1O could be employed in the visible to NIR photodetection. Moreover, the PL intensity increases with the thickness of single crystal, which is likely due to the higher absorption efficiency in thicker materials.

We firstly investigated the optoelectronic properties of the Y6-1O with a thickness of 108 nm. As shown in Fig. 2(a) and 2(b), the output and transfer curves of Y6-1O transistor revealed its n-type charge transport characteristics in its single crystal form, consistent with the previous report[38]. The resistance modulation through SiO_2 could reach as large as 10^4. The field effect electron mobility is calibrated to be 0.88 $cm^2V^{-1}s^{-1}$, which is much higher than that of thin film devices[38]. The enhanced carrier mobility is attributed to the long-range ordering of molecular arrangement within the single crystal. Fig. 2(c) shows the transfer characteristic curves under 638 nm laser illumination with different power intensities. A distinct photoresponse was evident in the Y6-1O single crystal phototransistor due to the photoconducting effect. As illustrated in Fig. 2(d), photons with energy higher than the bandgap (1.33 eV[41]) of the single crystal elicited an intrinsic photoresponse. The time resolved photoresponse is further measured by alternatively switching the laser on and off periodically. Fig. 2e shows the photoresponse for 405 nm and 638 nm laser under different intensity. The highest on/off ratio of the photocurrent could reach approximately 10^2 under strong incident light. The relationship between the photocurrent (I_{ph}) and incident intensity of light (P) follows a power law function, $I_{ph} \propto P^{\alpha}$, where α equals to 0.64 and 0.63 for 405 nm and 638 nm light, respectively. The relationship highlights the influence of photogenerated carrier generation and recombination dynamics[42-45]. According to previous reports[46], the coefficient α is near to one for the pure photoconducting effect in semiconductors. The deviation from the ideal value indicates the involvement of defects in the photoresponse process.

The photoresponse for different wavelengths from visible light to NIR (405 nm - 980 nm) of Y6-1O phototransistor has been further studied under different backgate voltages, as shown in Fig. 3(a)-(c). The dark current of the device decreases when backgate voltage changes from 40 V to -40 V, which is consistent with the trans-

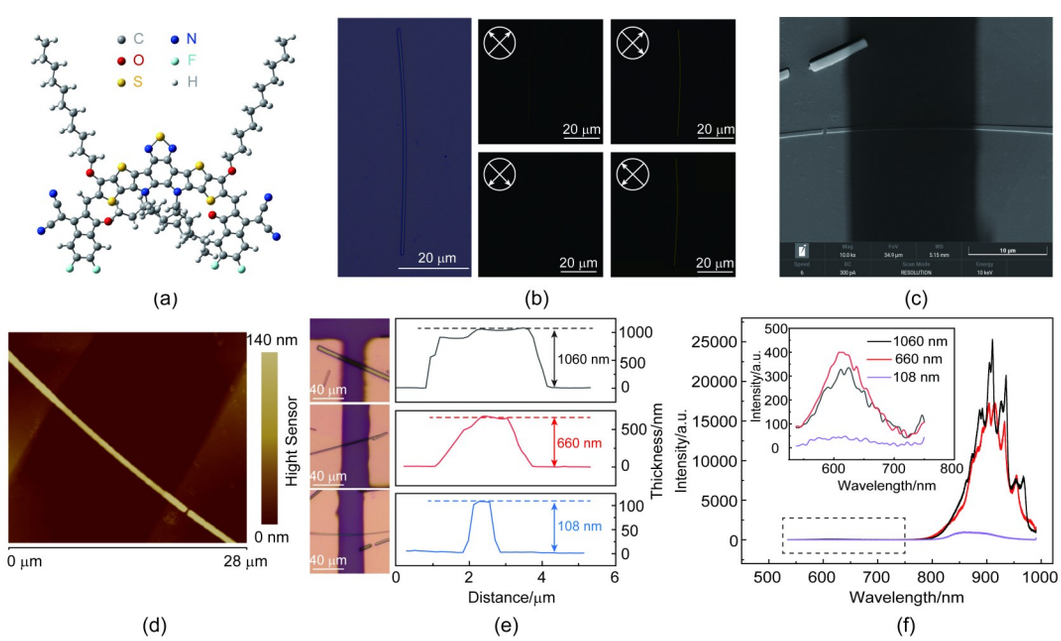

图 1　Y6-1O有机材料及表征分析:(a)具有高度共轭性的Y6-1O原子结构;(b)Y6-1O单晶的偏振光学显微镜图像(比尺:20 μm);(c)Y6-1O有机晶体管的场发射扫描电镜(SEM)图像;(d)Y6-1O有机晶体管的原子力显微镜(AFM)图像;(e)Y6-1O有机材料的厚度梯度及其光学图像;(f)1 060 nm、660 nm、106 nm厚度Y6-1O晶体的光致发光(PL)光谱响应

Fig. 1　Y6-1O organic semiconductor materials and characterization: (a) Y6-1O atomic structure with high conjugation; (b) Polarization optical microscope image of Y6-1O single crystal (scale: 20 μm), the arrows indicate the polarization of the incident and collected light; (c) Field emission scanning electron microscopy (SEM) images of Y6-1O organic transistors; (d) Atomic force microscopy (AFM) images of Y6-1O organic transistors; (e) Thickness profile of Y6-1O organic materials and their corresponding optical images; (f) photoluminescence (PL) spectral properties of Y6-1O crystals with 1 060 nm, 660 nm and 106 nm thickness

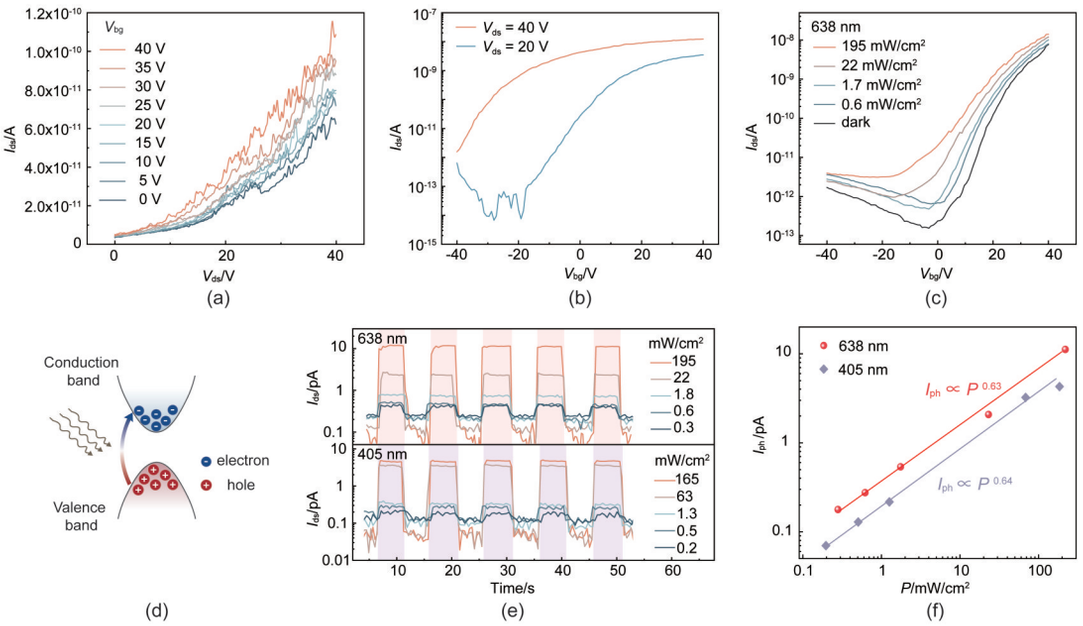

图2 106 nm厚Y6-1O单晶材料晶体管的光电特性：(a)不同偏置栅电压下的输出特性曲线；(b)不同漏源电压下的转移特性曲线；(c)638 nm不同功率密度下的转移特性曲线，V_{ds} = 40 V；(d)Y6-1O晶体光响应能带示意图；(e)Y6-1O晶体管在638 nm、405 nm入射光不同功率密度下的光响应，V_{ds} = 40 V；(f)638 nm、405 nm光照射下的光电流随入射光功率的函数关系

Fig. 2 Electrical and photoresponse of Y6-1O phototransistor with thickness of 106 nm: (a) Output characteristic curve at different bias gate voltages; (b) Transfer characteristic curves under different drain-source voltages; (c) Transfer characteristic curves at different power densities of 638 nm, V_{ds} = 40 V; (d) Schematic diagram of photoresponse band of Y6-1O crystal; (e) Photoresponse of Y6-1O transistor at different power densities of incident light at 638 nm and 405 nm, V_{ds} = 40 V; (f) The photocurrent of 638 nm and 405 nm irradiation as a function of the incident light power.

fer curves. Interestingly, the maximum photoresponse wavelength also changes with the backgate voltage (V_{bg}). The maximum photoresponse locates at 630 nm when V_{bg} = 40 V, but it changed to 785 nm when V_{bg} = -40 V. These results are thought to be related to the band diagram changes under gate voltages, as shown in Fig. 3 (d)-(f). On one hand, the gate voltage effectively modulate the electron density of the Y6-1O channel, resulting in the modulation of the dark current as well as the photocurrent. On the other hand, the fermi level of the Y6-1O is also regulated by the gate voltage, thereby adjusting the metal-semiconductor barrier at the electrode contacts. This is presumably related to the change of the maximum photoresponse wavelengths. The spectral response and responsivity under different backgate voltages are summarized in Fig. 3(g). As it can be seen, the net photocurrent and responsivity can be modulated three orders of magnitude by gate voltages. The maximum photoresponsivity is approximately 61.5 mA/W when V_{bg} = 40 V.

As aforementioned, the optical properties of Y6-1O are also influenced by the thickness of single crystal. Hence, we investigated the optoelectronic photoresponse for the device with thicker Y6-1O. Fig. 4(a) shows the photoresponse of Y6-1O with a thickness of 660 nm. We found the device shows higher photocurrent for wavelength from 405 nm to 850 nm when V_{bg} = 0 V comparing to the device made with 108 nm single crystal channel, while the dark current is still low. In particular, the photoresponse to the NIR (785 nm) gets enhanced. The photocurrent measured under different intensity of light are summarized in Fig. 4(b)(i). The photocurrent maitains a power law relationship with the intensity of incident light from 405 nm to 850 nm. The power coefficient α is estimated to be 0.87, which is superior comparing with the device made with thinner Y6-1O crystal, indicating the better crystal quality for thick nanoribbons. The maximum photoresponsivity is approximately 16.6 mA/W for 785 nm light (Fig. 4(b)(ii)). The comparison of the spectral photoresponse for both devices with different thicknesses (108 nm and 660 nm) is shown in Fig. 4(c). Firstly, we found that the photoresponse of the device made with 660 nm Y6-1O single crystal was significantly improved. And the peak photoresponse occurring in the NIR region, consistent with the absorption and PL properties of the Y6-1O single crystal. Additionally, a secondary peak photoresponse is observed at 520 nm in the visible region. In contrast, the device made with thinner (108 nm) Y6-1O single crystal exhibits a maximum photoresponse only in the visible region. Therefore, these findings suggest that Y6-1O single crystal hold promise for sensitive visible to NIR photodetection, with thicker samples show better performance in the NIR region.

3 Conclusions

In summary, we made the organic semiconductor

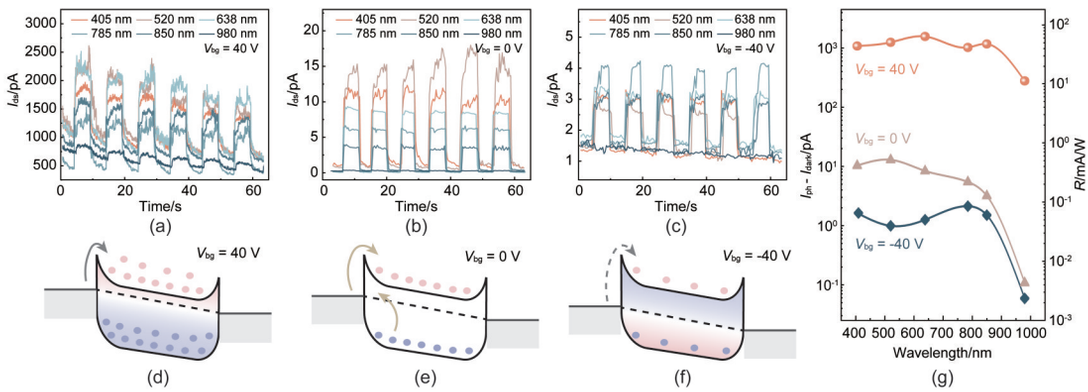

图 3　Y6-1O 不同栅压下的光响应行为：(a–c)不同栅压 40 V (a)、0 V (b)、−40 V (c)条件下器件对 400 nm 至 1 000 nm 波长光的响应，入射光功率 P = 10 mW/cm^2，V_{ds} = 40 V；(d–f)不同栅压条件下器件沟道材料能带结构图；(g)Y6-1O 晶体管在 40 V、0 V、−40 V 栅压下光电流和响应率与光波长关系

Fig. 3　Photoresponse of Y6-1O under different gate voltages: (a–c) The photoresponses for light from 400 nm to 1 000 nm under different gate voltages of 40 V (a), 0 V (b), and −40 V (c), when P = 10 mW/cm^2 and V_{ds} = 40 V; (d–f) Schematic of the band diagrams under gate voltage of 40 V (d), 0 V (e), and −40 V (f). (g) The spectral response of the Y6-1O phototransistor at different gate voltages.

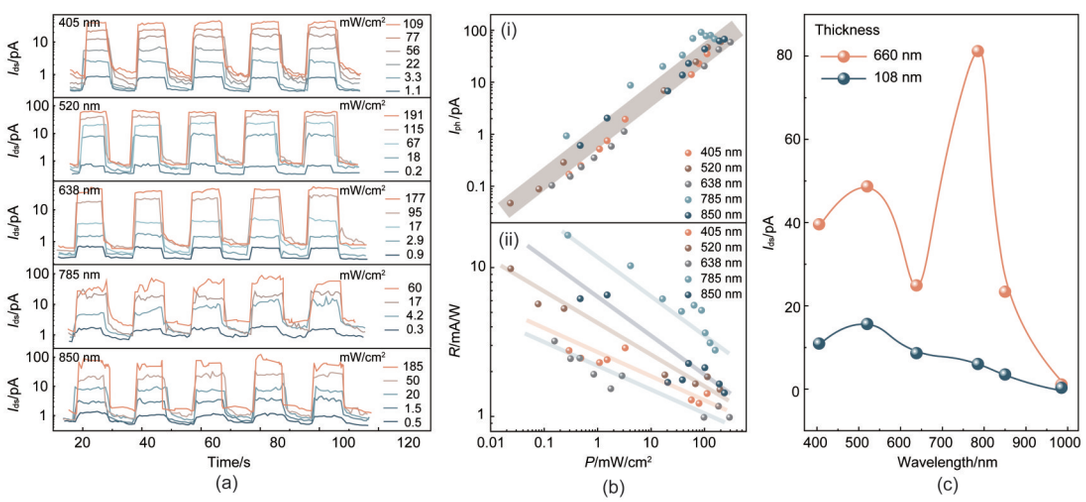

图 4　660 nm 厚 Y6-1O 晶体管的光响应：(a)器件对从 400 nm 至 1 000 nm 不同波长光的响应，其中 V_{ds} = 40 V，V_{bg} = 0 V；(b)(i)器件对不同波长光响应电流与入射光功率的关系；(b)(ii)器件对不同波长光响应率与入射光功率的关系；(c)不同厚度 Y6-1O 晶体管的光谱响应，P = 10 mW/cm^2

Fig. 4　Photoresponse of Y6-1O with thickness of 660 nm: (a) Photoresponse of the device for light from 400 nm to 1 000 nm, when V_{ds} = 40 V, V_{bg} = 0 V; (b) (i)The photocurrent and power density relationship for different wavelengths. (b) (ii) The photo responsivity and power density relationship for different wavelengths. (c)The spectral response of Y6-1O phototransistors for different thicknesses (108 nm, 660 nm) when P=10 mW/cm^2

single crystal Y6-1O through the convenient droplet casting method. Polarized optical microscopy revealed the high-quality single crystal structure of Y6-1O, while PL properties suggest its suitability for use in NIR optoelectronic devices. Phototransistors based on Y6-1O with different thicknesses were thoroughly investigated. These devices exhibit low dark current and high photoresponsivity across the visible to NIR spectrum, with the peak photoresponse observed in the NIR region. Moreover, the spectral response of the Y6-1O photodetector could be tuned by adjusting both the gate voltage and the thickness of the sample. In particular, the device made with 660-nm-thick Y6-1O single crystal shows photoresponsivity of 16.6 mA/W for 785 nm light, and shows strong potential in application in the visible to NIR photodetection. Ultimately, this work highlights an alternative approach of developing novel NIR photodetectors using the organic semiconducting single crystals. Such devices hold promise for various applications including night vision monitoring, biomedical imaging, environmental monitoring, and wearable devices owing to their low cost, scalability, and flexibility characteristics.

References

[1] Kazunori Kuribara, Atsushi Takei, Takashi Sato, *et al*. Device Physics of Solution-Processed Organic Field-Effect Transistors [J]. *Ad-*

vanced Materials, 2005, **17**(20): 2411-2425.
[2] Antonio Facchetti. Semiconductors for organic transistors [J]. *Materials Today*, 2007, **10**(3): 28-37.
[3] GENG Di, WANG Kai, LI Ling, *et al*. Thin-film transistors for large-area electronics [J]. *Nature Electronics*, 2023, **6**(12): 963-972.
[4] Mirshojaeian Hosseini M J, Yang Y, Kruger W, *et al*. 270 nm ultra-thin self-adhesive conformable and long-term air-stable complimentary organic transistors and amplifiers [J]. *npj Flexible Electronics*, 2023, **7**(1): 38.
[5] Mohammad Javad Mirshojaeian Hosseini, Yi Yang, Walter Kruger, *et al*. Device Physics of Solution-Processed Organic Field-Effect Transistors [J]. *Advanced Materials*, 2005, **17**(20): 2411-2425.
[6] GUAN Ying-Shi, QIAO Jing, LIANG Ying-Ying, *et al*. A high mobility air-stable n-type organic small molecule semiconductor with high UV - visible-to-NIR photoresponse [J]. *Light: Science & Applications*, 2022, **11**(1): 236.
[7] Haechan Park, Sehyun Kim, Lee Juyeong, *et al*. Organic flexible electronics with closed-loop recycling for sustainable wearable technology [J]. *Nature Electronics*, 2023, **7**(1): 39-50.
[8] ZHONG Dong-Lai, WU Can, JIANG Yuan-Wen, *et al*. High-speed and large-scale intrinsically stretchable integrated circuits [J]. *Nature*, 2024, **627**(8003): 313-320.
[9] Rak Hwan Kim, Dae Hyeong Kim, Xiao Jianliang, *et al*. Waterproof AlInGaP optoelectronics on stretchable substrates with applications in biomedicine and robotics [J]. *Nature Materials*, 2010, **9**(11): 929-937.
[10] Naoji Matsuhisa, Simiao Niu, Stephen J. K. O'Neill, et al. High-frequency and intrinsically stretchable polymer diodes [J]. *Nature*, 2021, **600**(7888): 246-252.
[11] LIU Kai, OUYANG Bang, GUO Xiao-Jun, *et al*. Advances in flexible organic field-effect transistors and their applications for flexible electronics [J]. *npj Flexible Electronics*, 2022, **6**(1): 187.
[12] Matthew S. White, Martin Kaltenbrunner, Eric D. Głowacki, et al. Ultrathin, highly flexible and stretchable PLEDs [J]. *Nature Photonics*, 2013, **7**(10): 811-816.
[13] Minwoo Nam, Jaehyeock Chang, Hagseon Kim, *et al*. Highly reliable and stretchable OLEDs based on facile patterning method: toward stretchable organic optoelectronic devices [J]. *npj Flexible Electronics*, 2024, **8**(1): 17.
[14] Eun Gyo Jeong, Jeong Hyun Kwon, Ki Suk Kang, *et al*. A review of highly reliable flexible encapsulation technologies towards rollable and foldable OLEDs [J]. *Journal of Information Display*, 2019, **21**(1): 19-32.
[15] Sung-Min Lee, Jeong Hyun Kwon, Seonil Kwon, *et al*. A Review of Flexible OLEDs Toward Highly Durable Unusual Displays [J]. *IEEE Transactions on Electron Devices*, 2017, **64**(5): 1922-1931.
[16] Hao Ren, Jing-De Chen, Yan-Qing Li, *et al*. Recent Progress in Organic Photodetectors and their Applications [J]. *Advanced Science*, 2020, **8**(1): 2002418.
[17] MIAO Jian-Li, ZHANG Fu-Jun. Recent Progress on Photomultiplication Type Organic Photodetectors [J]. *Laser & Photonics Reviews*, 2018, **13**(2): 1800204.
[18] Ross D. Jansen-van Vuuren, Ardalan Armin, Ajay K. Pandey, et al. Organic Photodiodes: The Future of Full Color Detection and Image Sensing [J]. *Advanced Materials*, 2016, **28**(24): 4766-4802.
[19] YANG De-Zhi, MA Dong-Ge. Development of Organic Semiconductor Photodetectors: From Mechanism to Applications [J]. *Advanced Optical Materials*, 2018, **7**(1): 1800522.
[20] QIN Jian-Qiang, LAN Lin-Kai, Chen Shanshan, *et al*. Recent Progress in Flexible and Stretchable Organic Solar Cells [J]. *Advanced Functional Materials*, 2020, **30**(36): 2002529.
[21] Neal R. Armstrong, Wang Weining, Dana M. Alloway, *et al*. Organic/Organic′ Heterojunctions: Organic Light Emitting Diodes and Organic Photovoltaic Devices [J]. *Macromolecular Rapid Communications*, 2009, **30**(9-10): 717-731.
[22] CAO Wei-Ran, XUE Jian-Geng. Recent progress in organic photovoltaics: device architecture and optical design [J]. *Energy & Environmental Science*, 2014, **7**(7): 2123-2144.
[23] Diogenes Placencia, Wang Weining, R. Clayton Shallcross, *et al*. Organic Photovoltaic Cells Based On Solvent-Annealed, Textured Titanyl Phthalocyanine/C60 Heterojunctions [J]. *Advanced Functional Materials*, 2009, **19**(12): 1913-1921.
[24] Havid Aqoma, Sujung Park, Hye-Yun Park, *et al*. 11% Organic Photovoltaic Devices Based on PTB7-Th: PC71BM Photoactive Layers and Irradiation-Assisted ZnO Electron Transport Layers [J]. *Advanced Science*, 2018, **5**(7): 1700858.
[25] Scott A. Mauger, Melodie P. Glasser, Bertrand J. Tremolet de Villers, et al. Doped Interlayers for Improved Selectivity in Bulk Heterojunction Organic Photovoltaic Devices [J]. *Advanced Materials Interfaces*, 2015, **3**(2): 1500346.
[26] LI Ding, YI Zi-Di, Wang Xiao-Ye, *et al*. Polymer Semiconductors: Synthesis, Processing, and Applications [J]. *Chemical Reviews*, 2023, **123**(12): 7421-7497.
[27] MEI Jian-Guo, DIAO Ying, Anthony L. Appleton, *et al*. Integrated Materials Design of Organic Semiconductors for Field-Effect Transistors [J]. *Journal of the American Chemical Society*, 2013, **135**(18): 6724-6746.
[28] Antonio Facchetti. π-Conjugated Polymers for Organic Electronics and Photovoltaic Cell Applications [J]. *Chemistry of Materials*, 2010, **23**(3): 733-758.
[29] Oksana Ostroverkhova. Organic Optoelectronic Materials: Mechanisms and Applications [J]. *Chemical Reviews*, 2016, **116**(22): 13279-13412.
[30] AN Xiang, WEI Chuan-Xin, BAI Lu-Bing, *et al*. Photoexcitation dynamics and energy engineering in supramolecular doping of organic conjugated molecules [J]. *Light: Science & Applications*, 2023, **12**(1): 30.
[31] Hwan-Hee Cho, Daniel G. Congrave, Alexander J. Gillett, *et al*. Suppression of Dexter transfer by covalent encapsulation for efficient matrix-free narrowband deep blue hyperfluorescent OLEDs [J]. *Nature Materials*, 2024, **23**(1): 519-526.
[32] CUI Yong, YAO Hui-Feng, ZHANG Jian-Qi, *et al*. Over 16% efficiency organic photovoltaic cells enabled by a chlorinated acceptor with increased open-circuit voltages [J]. *Nature Communications*, 2019, **10**(1): 2515.
[33] CUI Yong, XU Ye, YAO Hui-Feng, *et al*. Single-Junction Organic Photovoltaic Cell with 19% Efficiency [J]. *Advanced Materials*, 2021, **33**(41): 2102420.
[34] CUI Yong, YAO Hui-Feng, ZHANG Jian-Qi, *et al*. Single-Junction Organic Photovoltaic Cells with Approaching 18% Efficiency [J]. *Advanced Materials*, 2020, **32**(19): 1908205.
[35] LI Shui-Xing, LI Chang-Zhi, SHI Min-Min, *et al*. New Phase for Organic Solar Cell Research: Emergence of Y-Series Electron Acceptors and Their Perspectives [J]. *ACS Energy Letters*, 2020, **5**(5): 1554-1567.
[36] LIU Qi-Shi, JIANG Yu-Fan, JIN Ke, *et al*. 18% Efficiency organic solar cells [J]. *Science Bulletin*, 2020, **65**(4): 272-275.
[37] ZHAN Ling-Ling, LI Shui-Xing, Tsz-Ki Lau, *et al*. Over 17% efficiency ternary organic solar cells enabled by two non-fullerene acceptors working in an alloy-like model [J]. *Energy & Environmental Science*, 2020, **13**(2): 635-645.
[38] CHEN Yu-Zhong, WU Zeng, DING Lu, *et al*. Manipulating Crystal Stacking by Sidechain Engineering for High-Performance N-Type Organic Semiconductors [J]. *Advanced Functional Materials*, 2023, **33**(50): 2304316.
[39] XIE Bo-Ming, CHEN Zhong-Xin, YING Lei, *et al*. Near-infrared organic photoelectric materials for light-harvesting systems: Organic photovoltaics and organic photodiodes [J]. *InfoMat*, 2019, **2**(1): 57-91.
[40] MENG Dong, ZHENG Ran, ZHAO Ye-Pin, *et al*. Near-Infrared Materials: The Turning Point of Organic Photovoltaics [J]. *Advanced Materials*, 2022, **34**(10): 2107330.
[41] YUAN Jun, ZHANG Yun-Qian, ZHOU Liu-Yang, *et al*. Single-Junction Organic Solar Cell with over 15% Efficiency Using Fused-Ring Acceptor with Electron-Deficient Core [J]. *Joule*, 2019, **3**(4): 1140-1151.
[42] A. J. Mozer, G. Dennler, N. S. Sariciftci, *et al*. Time-dependent mobility and recombination of the photoinduced charge carriers in conjugated polymer/fullerene bulk heterojunction solar cells [J]. *Physical Review B*, 2005, **72**(3): 035217.
[43] Armantas Melianas, Fabian Etzold, Tom J. Savenije, *et al*. Photo-generated carriers lose energy during extraction from polymer-fullerene solar cells [J]. *Nature Communications*, 2015, **6**(1): 8778.
[44] Seiichiro Izawa, Masahiro Hiramoto. Efficient solid-state photon upconversion enabled by triplet formation at an organic semiconductor interface [J]. *Nature Photonics*, 2021, **15**(12): 895-900.
[45] Yuji Sakamoto, Seiichiro Izawa, Hideo Ohkita, *et al*. Triplet sensitization via charge recombination at organic heterojunction for efficient near-infrared to visible solid-state photon upconversion [J]. *Communications Materials*, 2022, **3**(1): 76.
[46] Sandro Rao, Elisa D. Mallemace, Giuliana Faggio, *et al*. Experimental characterization of the thermo-optic coefficient vs. temperature for

4H-SiC and GaN semiconductors at the wavelength of 632 nm [J]. *Scientific Reports*, 2023, **13**(1): 10205.